8th U. S. National Combustion Meeting
Organized by the Western States Section of the Combustion Institute
and hosted by the University of Utah
May 19-22, 2013

Alternate Fuel Combustor Operated on Glycerol and Methane

Lulin Jiang, Ajay K. Agrawal and Robert P. Taylor

Department of Mechanical Engineering, University of Alabama,
Tuscaloosa, Alabama 35401, USA

Abstract

Disposal of glycerol, the byproduct from biodiesel production, is an emerging issue with the increasing interest in utilizing fuels produced from biomass. Glycerol and other industrial waste products with moderate amounts of stored chemical energy can be economically viable alternative fuels because of their low cost. Previous research has shown that glycerol is combustible, in spite of its high ignition temperature, by preheating the combustion zone with propane or methane. We have reported that glycerol with its extraordinarily high kinematic viscosity can still be finely atomized by the so-called flow blurring (FB) injector to produce clean flames with extremely low emissions at the combustor exit. In the present study, a fuel-flexible combustor with a FB injector is utilized to simultaneously burn liquid and gaseous fuels. Measurements of product gas temperature and CO and NO_x emissions are acquired at various axial and transverse locations inside a swirl-stabilized combustor to illustrate the flame structure. For a fixed heat release rate (HRR), methane and glycerol flow rates are varied to vary the percentages of HRR from each fuel and thus, the fuel mix. For a fixed fuel mix, the air-to-liquid mass ratio (ALR) through the injector is varied to investigate its effect on the flame structure. Results show low-emissions with combustion of glycerol without and with methane supply. The addition of methane improves glycerol combustion by improving fuel vaporization, fuel-air mixing, and fuel oxidation resulting in localized zones of higher product gas temperatures. CO emissions decrease and NO_x emissions increase when increasing the percentage of HRR from methane. Higher ALR improves atomization to form smaller droplets that vaporize rapidly and result in shorter primary reaction zone with higher local temperatures reducing CO emissions and increasing NO_x emissions. In spite of these differences, all fuel combinations result in complete combustion with extremely low CO and NO_x emissions at the combustor exit.

1. Introduction

Disposal of glycerol, the byproduct from biodiesel production, is an emerging issue with the increasing interest in utilizing fuels produced from biomass. About 1 kg of crude glycerol is generated for 9 kg of biodiesel produced [1]. Even though pure glycerol finds applications in food, cosmetics and pharmaceutical industries, it is too costly for biodiesel producers to refine crude glycerol into high purity glycerol. Therefore, glycerol generated during biodiesel production is often considered a waste product causing environmental problems. Conversion of glycerol into value added products and chemicals has been studied in recent years. For instance, glycerol could be blended with gasoline to recover some of its chemical energy in the form of an alternative fuel [2]. Glycerol is an attractive feedstock for producing chemicals such as 1, 3-propanediol with end uses into corterra polymers, UV-Cured coatings, solvents and anti-freeze, etc [3, 4]. Using Enterobacter

Aerogenes HU-101 to convert glycerol into fuels such as hydrogen and ethanol has been studied for future portfolio of alternative fuels [5]. While the previous research offers routes to convert glycerol into useful products, significant cost and energy is still required. For example, anaerobic digestion of glycerol recovers only 11.93 MJ/kg out of around 16 MJ/kg energy in glycerol [6].

Previous research has shown that glycerol is combustible, in spite of its high ignition temperature and high kinematic viscosity at the room temperature. Thus, direct combustion of glycerol can be an economically viable solution to effectively utilize glycerol to meet our energy needs. Recently, McNeil et al. [7] tested glycerol combustion in a compression ignition engine by supplying air at above 90°C and glycerol at around 144°C to decrease viscosity and overcome the high ignition temperature characteristic of glycerol. The results showed low emissions of CO, NO_x, and particulates, and low emissions of carbonyl such as acrolein from glycerol operation than equivalent engines operating on diesel or biodiesel fuel. Glycerol fuel also improved the stability over the engine operation increasing catalyst efficiency and lowering the chance of catalytic degradation. Direct combustion of glycerol resulted in 2.3 time greater heat recovery than the anaerobic digestion process. This study suggested that engine operation with glycerol would comply with the strictest emission standards for many years to come such the proposed 2015 Tier 4 Californian Emissions Standards.

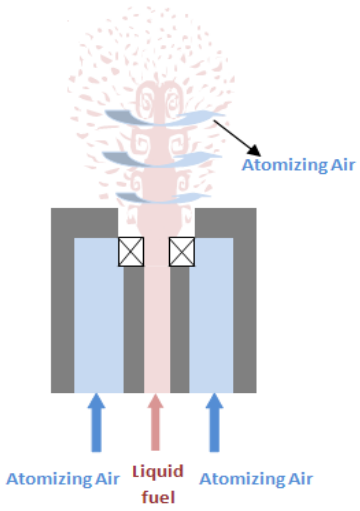

Fig. 1 Diagram of siphon air atomizing nozzle.

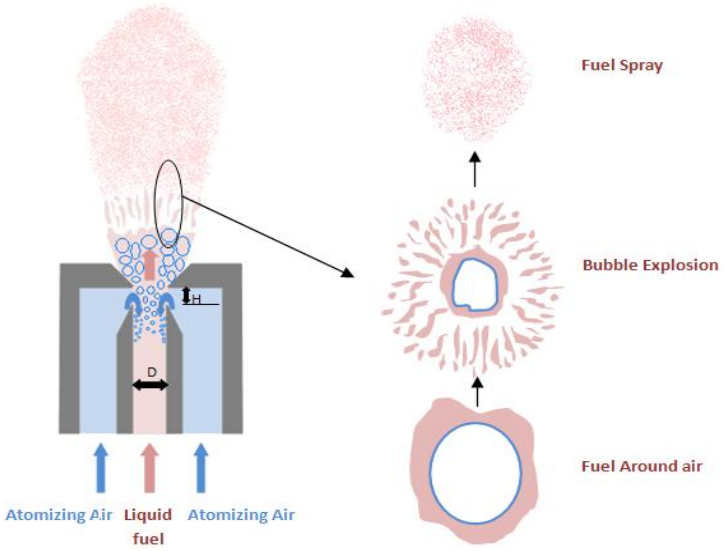

Fig. 2 Working principle of the flow blurring injector

For continuous flow applications such as gas turbines and burners, previous research has shown that glycerol can be successfully combusted. Metzger [8] used a Delavan Siphon type SNA Air-Blast (AB) atomizer to form glycerol spray at room temperature using pressurized air. A liquid fuel pump was used to pump the glycerol and a much higher flow rate of air was necessary compared to that needed to atomize kerosene or diesel. Likewise, Myles et al. [9] used an air-assist atomizer (Delavan model 30609-3) to create glycerol spray. In this study, glycerol was preheated to 93°C and atomizing air was preheated to 150°C before the two fluids were supplied to the fuel injector. Preheating glycerol can dramatically decrease its viscosity to levels similar to conventional fuel oils, which is highly beneficial to create a fine spray. However, AB injector is not ideal for glycerol and other highly viscous fuels because of the high energy input required to supply large amounts of pressurized air for atomization; Figure 1 shows the working principle of AB atomizer, whereby high velocity airflow is introduced from the injector to destabilize the shear layer of the fuel jet, which

can result in a spray with fine droplets. However, the shear layer instabilities are suppressed by high kinematic viscosity of the fuel, which limits the ability of the AB injector to produce a fine spray [10].

Another kind of fuel injector, flow-blurring (FB) injector, was used by Benjamin et al. [10]. Gañán-Calvo [11] first reported that for a set atomizing air flow rate, the FB injection concept created "five to fifty times" more fuel surface area than a plain-jet AB atomizer. This injection method utilizes two-phase flow concept to create the spray. The injection principle shows in Figure 2 [12] consists of a fuel tube and an exit orifice both of diameter, D and a gap of height H between the fuel tube tip and the orifice. If the ratio H/D is less than 0.25, the atomizing air bifurcates as it reaches the gap between exit orifice and the fuel tube tip. A portion of the air flows into the fuel tube, while the rest leaves the injector through the orifice. The turbulent two-phase flow created inside the fuel tube, then leaves the injector through the orifice. Significant decrease of pressure in the orifice cases air bubbles to expand and break apart the surrounding liquid into fine droplets. Previous studies have shown that FB injector provides finer spray with lower energy input since it incurs a lower pressure drop in the atomizing air line [13-14]. Liquid fuel atomized by FB atomizer burns in lean premixed (LPM) mode and thus yields lower CO and NOx emissions [12, 15-16]. Previous research by our group has proven that in spite of high kinematic viscosity, glycerol can be finely atomized by FB injector. Glycerol has a high ignition temperature and has to be combusted in the combustion zone with very high temperature to get stable flame. In spite of these challenges, very low emissions at the combustor exit have been reported when using glycerol with FB atomizer [17].

Prior studies have demonstrated combustor operation with glycerol including emissions reported at the exit plane only. In this research, a similar alternative fuel combustor with FB injector is used with the purpose of documenting gas temperature and emissions at various axial and radial locations inside the combustor to illustrate the flame structure. For a fixed heat release rate (HRR), different amounts of glycerol and methane are introduced to simultaneously combust both fuels. For a fixed fuel mix and total air flow rate, the effect of the air-to-liquid mass ratio (ALR) on the flame structures is investigated by varying the atomizing air flow rate. The following sections describe the experimental section following by results and conclusions.

2. Experimental setup

Fig. 3(a) shows the schematic of the experimental setup. After passing through filters and water traps, the compressed air is separated into primary air and atomizing air lines. Primary air enters the mixing channel through the plenum filled with marbles to breakdown large vortical structures. Methane is introduced into the mixing channel, and the fuel-air mixture or primary air pass through a section filled with steel wool to further homogenize the flow. This flow is introduced into the combustor through a swirler with axial curved vanes at 30 degree angle with respect to the transverse plane and swirl number of approximately 1.5. The fuel injector consists of a central fuel port with sidewise fuel inlet attachment and multiple openings around the peripheral region to introduce the atomizing air. Liquid fuel enters the injector via tubing connected with the injector holder and atomizing air is supplied from the bottom of the injector holder. The FB injection concept is implemented by placing a spacer of width $H = 0.25D$ between the fuel tube tip and injector discharge orifice as shown in Fig. 2. In this study, D = 0.5 mm and $H = 0.375$ mm.

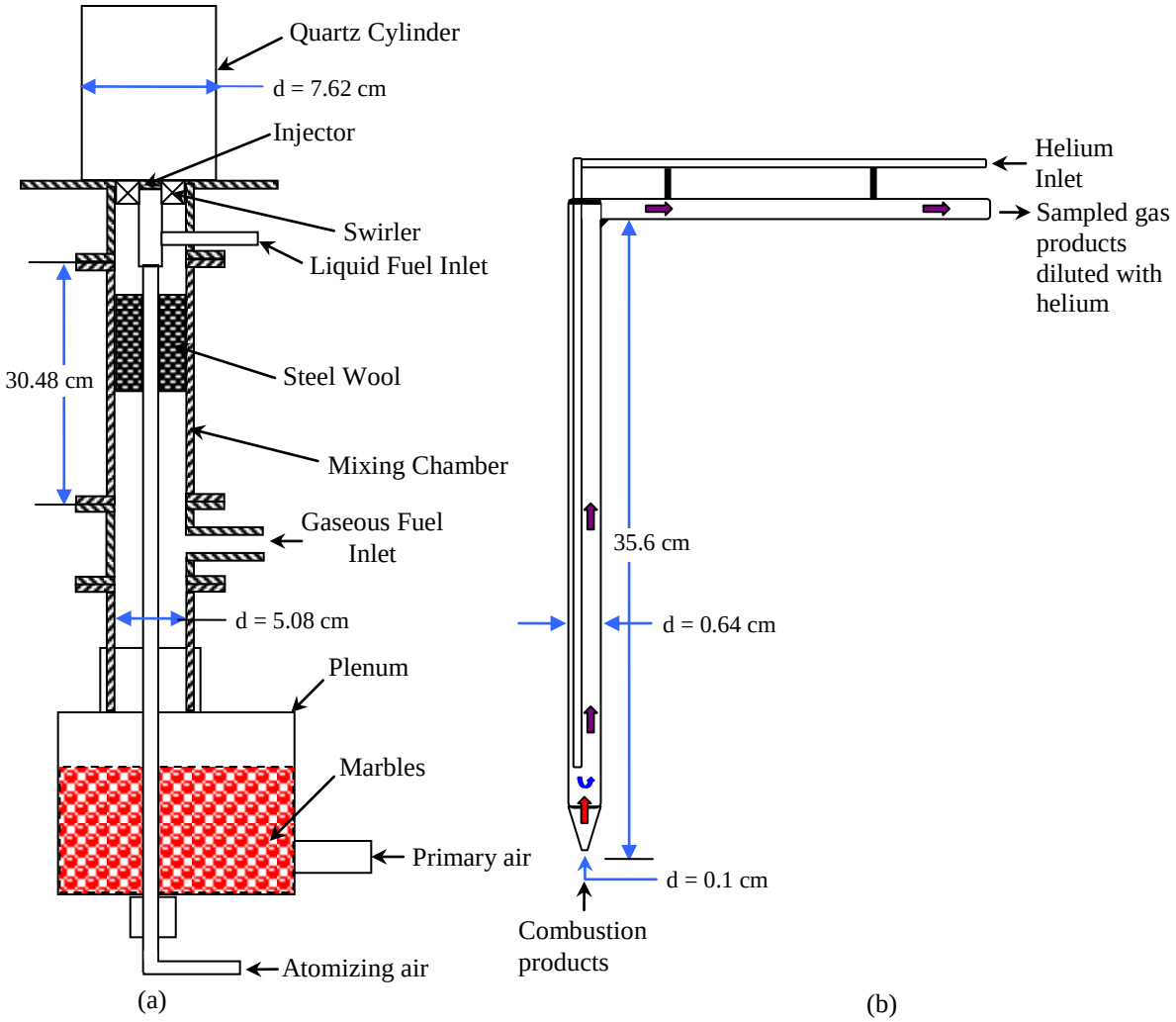

Fig. 3 (a) Experimental Setup Schematic and (b) Helium cooled sampling probe.

Mass flow rates of air and methane are controlled by Sierra Smart Track 2 Series 100 mass flow controllers with accuracy of ± 1% of the reading. Liquid fuel is supplied by a Cole Parmer high performance peristaltic metering pump (Model 7523-90) with an accuracy of ± 0.25% of the reading.

For characterizing the combustion products, R-type thermocouple insulated by ceramic tubes to minimize axial heat conduction was used to measure gas temperatures up to 2000 K. The thermocouple wire diameter was 0.25 mm and the bare bead diameter was 1.5 mm. The thermocouple temperature correction for radiation was estimated by using bead emissivity of 0.2 and air properties to approximate properties of the combustion products. The temperature distribution on the external surface of the quartz combustor was measured by an infrared camera (FLIR-T620) calibrated for temperature up to 2000 K. Free convection coefficient of 12 W/m^2-K for air was used to calculate the heat loss through the outside wall of the combustor. The CO and NOx emissions were measured using a Nova model 376WP gas analyzer with accuracy of ± 2 ppm. For enabling accurate measurements inside the flame zone, an in-house built, helium-cooled emission probe illustrated in Fig. 3(b) was utilized. This probe is made of two coaxial quartz tubes that enable mixing of combustion products and helium in the outer tube. Helium with its high specific heat

capacity reduces the temperature of the sampled combustion products to quench reactions near the probe tip. The helium flow rate is controlled by a needle valve to ensure that it does not exit through the probe tip to adversely affect the flame structure. The helium concentration in the sampled products was approximately 20% (by volume), and it was measured by a real-time Airsense High Speed Multi-component Gas Analyzer with accuracy of ± 2%. The sampled data were corrected for helium dilution and are reported as such. Gas temperatures and emissions measurements were taken at 10 axial planes with 11 transverse data at each axial plane. Transverse coordinate is defined as y-axis with the center at the axis of the combustor axis. Axial coordinate is defined as z-axis with the flow direction as the positive direction, and origin located at the dump plane of the combustor.

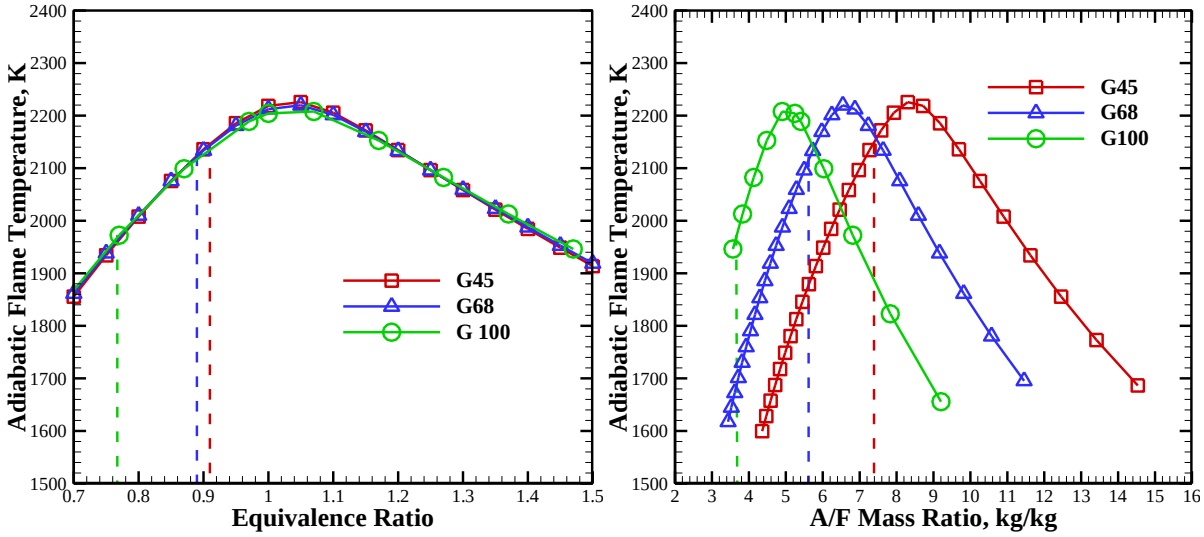

Fig. 4 Adiabatic flame temperatures as the function of (a) equivalence ratio and (b) air to fuel mass ratio.

The experiment is started with pure methane combustion to preheat the system and then, glycerol is gradually introduced into the combustion system through the FB injector. The total airflow rate, including primary airflow rate through the swirler and atomizing air through the injector, is kept constant at 150 standard liters per minute (slpm). For HRR = 7.9kW, the effect of air to liquid mass ratio is investigated for ALR = 1.47 and 2.23, for two fuel mixes, G45 and G68, where G45 signifies that 45% of the HRR is from glycerol and the rest is from methane. G100 case with HRR = 7 kW is also investigated for ALR = 1.13, which pertains to the cleanest glycerol flame conditions. G45, G68 and G100 fuel mix represents equivalence ratio of 0.91, 0.89 and 0.77, respectively. The Chemkin-pro software was used to compute the adiabatic flame temperature (T_{ad}) at equilibrium for the experimental conditions listed above, shown in Fig. 4. The computed T_{ad} is 2147 K, 2122 K and 1972 K, respectively, for G45, G68 and G100. Note that T_{ad} represents temperature achieved with complete combustion without heat loss from the combustor wall. However, the quartz combustor used in the present study results in unavoidable heat loss, which can be significant. In addition, the local flame temperature in the liquid fuel flame is related to the local equivalence ratio determined by fuel atomization processes affecting fuel droplet diameter, fuel pre-vaporization, and fuel-air mixing processes, which vary greatly throughout the combustor.

3. Results and discussions

3.1. Effect of Methane Addition

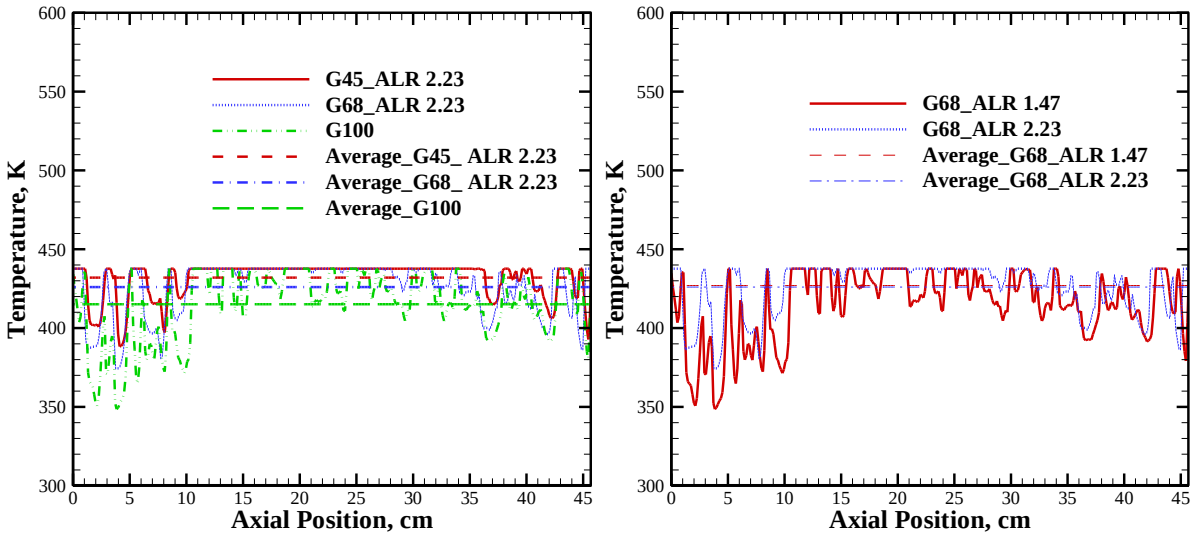

(a) (b)

Fig. 5 Surface Temperatures of the insulated combustor for (a) fuel composition and (b) ALRs.

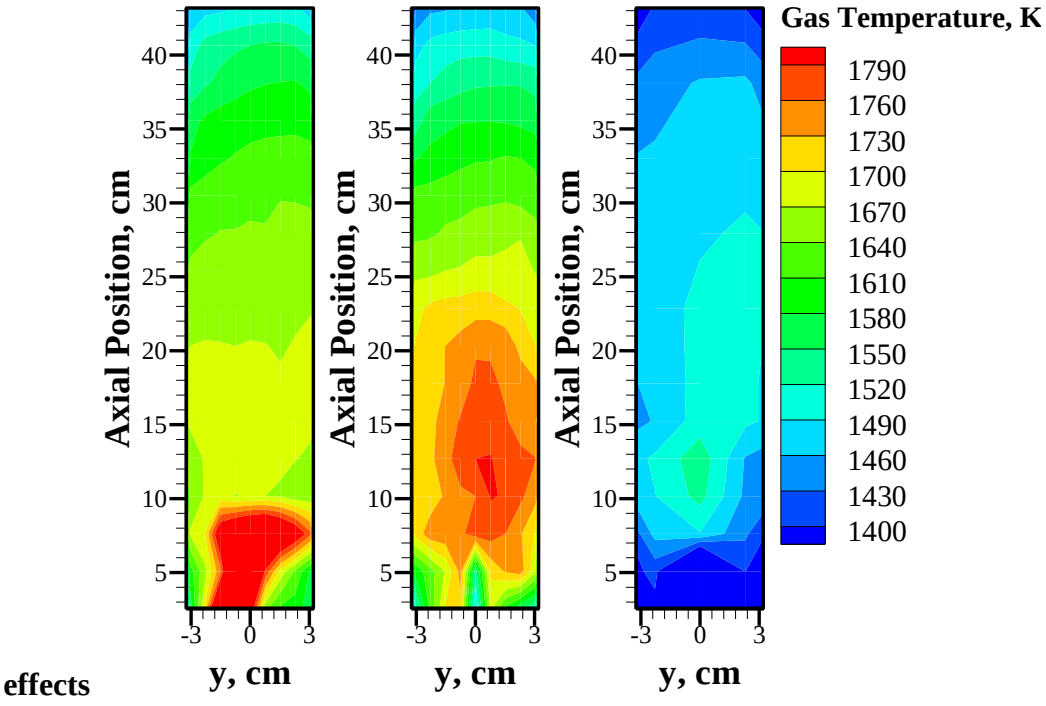

effects

(a) (b) (c)

Fig. 6 Gas temperature contour inside the combustor for (a) G45_ALR 2.23, and (b) G68_ALR 2.23 (c) G100.

Fig. 5(a) shows the axial profile of the surface temperature of the insulated combustor for G45, G68, and G100 flames. The average surface temperature is 432 K and 426 K respectively for G45, G68 flames and slightly lower (415) K for G100 flame. This plot helps in estimating heat loss from combustor to surroundings. Mean surface temperature close to the injector where fuel pre-vaporization and fuel-air mixing take place is slightly lower. The mean surface temperature is higher for z between 10 cm and 35 mm and it similar for all the three cases indicating relatively minor effects of the fuel mix. For z > 35 cm, the decrease in wall temperature is indicative of the heat loss to the ambient by natural convection and radiation.

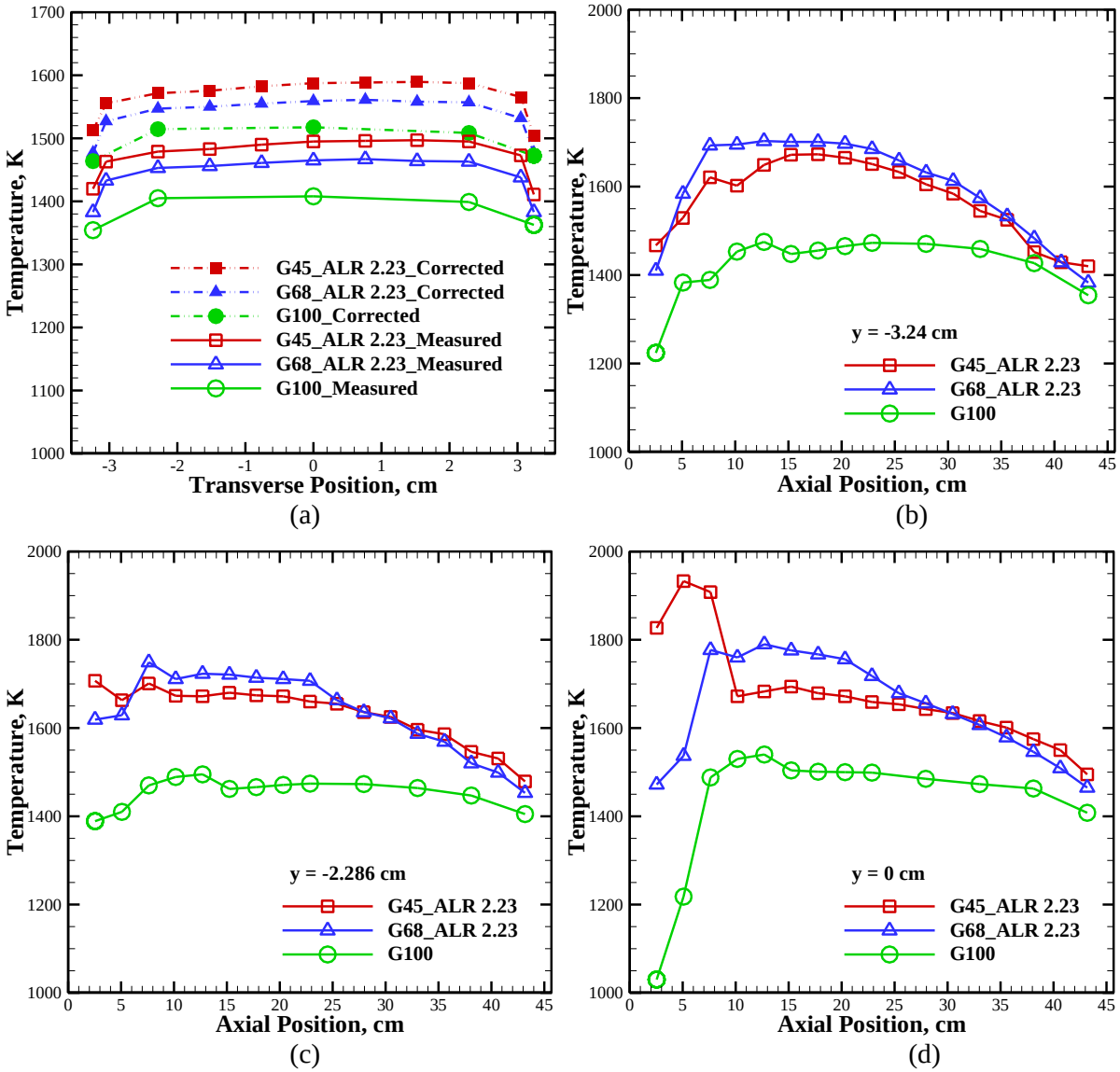

Fig. 7 Gas temperatures in the combustor for different fuel composition.

Fig. 6 shows contours of temperatures (uncorrected) inside the combustor for the flames with different fuel fix. For G45 flame, the reaction zone is closer to the injector exit where the temperature is highest. The reaction zone shifts downstream for G68 flame and a rather distributed reaction zone is observed for the G100 flame. These differences in the reaction zone location are attributed to the residence time needed to fully vaporize the liquid fuel. Methane combustion is expected to improve vaporization of glycerol spray, which results in a shorter reaction zone. In

contrast, G100 flame requires a greater distance to fully vaporize and combustion the fuel, which results in a longer, but low temperature reaction zone. Downstream of the reaction zone, the product gas temperature decreases because of the heat loss to the ambient as discussed above.

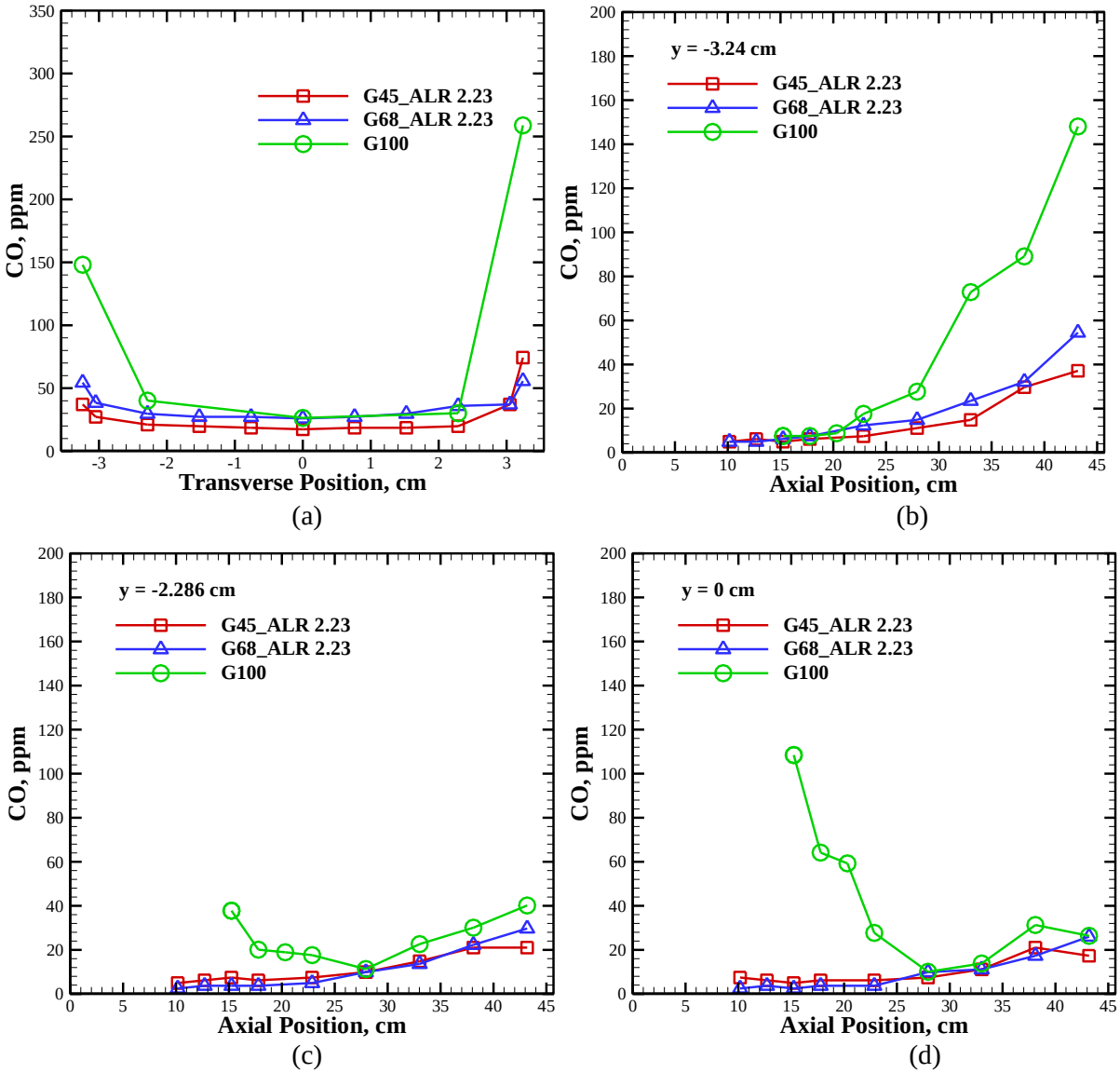

Fig. 8 CO concentrations in the combustor for different fuel composition.

Fig. 7(a) illustrates transverse profiles of product gas temperature at the combustor exit plane. Both uncorrected and radiation-corrected temperature data are presented, with corrections ranging from 90 K to 110K. Profiles show slightly higher temperature in the center of the combustor and temperature decreasing towards the wall because of the heat loss. For G45 and G48 fuel mixes, the HRR is the same (7.9 kW) which results in similar exit temperature profiles signifying complete combustion and/or minor effects of fuel mix on combustion. For G100, the HRR is slightly smaller (7.0 kW) and hence, product gas temperature at the combustor is also smaller than the previous two cases. Figs. 7(b)-(d) show axial profiles of gas temperature at three radial locations in the combustor. For G68 and G100 flames, a lower temperature is observed in the near injector region where fuel pre-vaporization zone and fuel-air mixing take place. Peak temperatures are observed in

the reaction zone where majority of the heat is released. At locations closer to the combustor exit, heat loss from the combustor exceeds any heat release by secondary reactions and thus, the temperature decrease in the flow direction. Matching axial profiles indicate that the differences in the fuel mix are confined to the near injector region, and that the fuel combust similarly with good glycerol pre-vaporization and fuel-air mixing. As discussed before, G45 and G68 flames are more intense compared to the G100 flame with an extended reaction zone. For G45 and G68 flames, heat released from methane combustion increases the temperature in the near field and provides thermal feedback for faster pre-vaporization of glycerol.

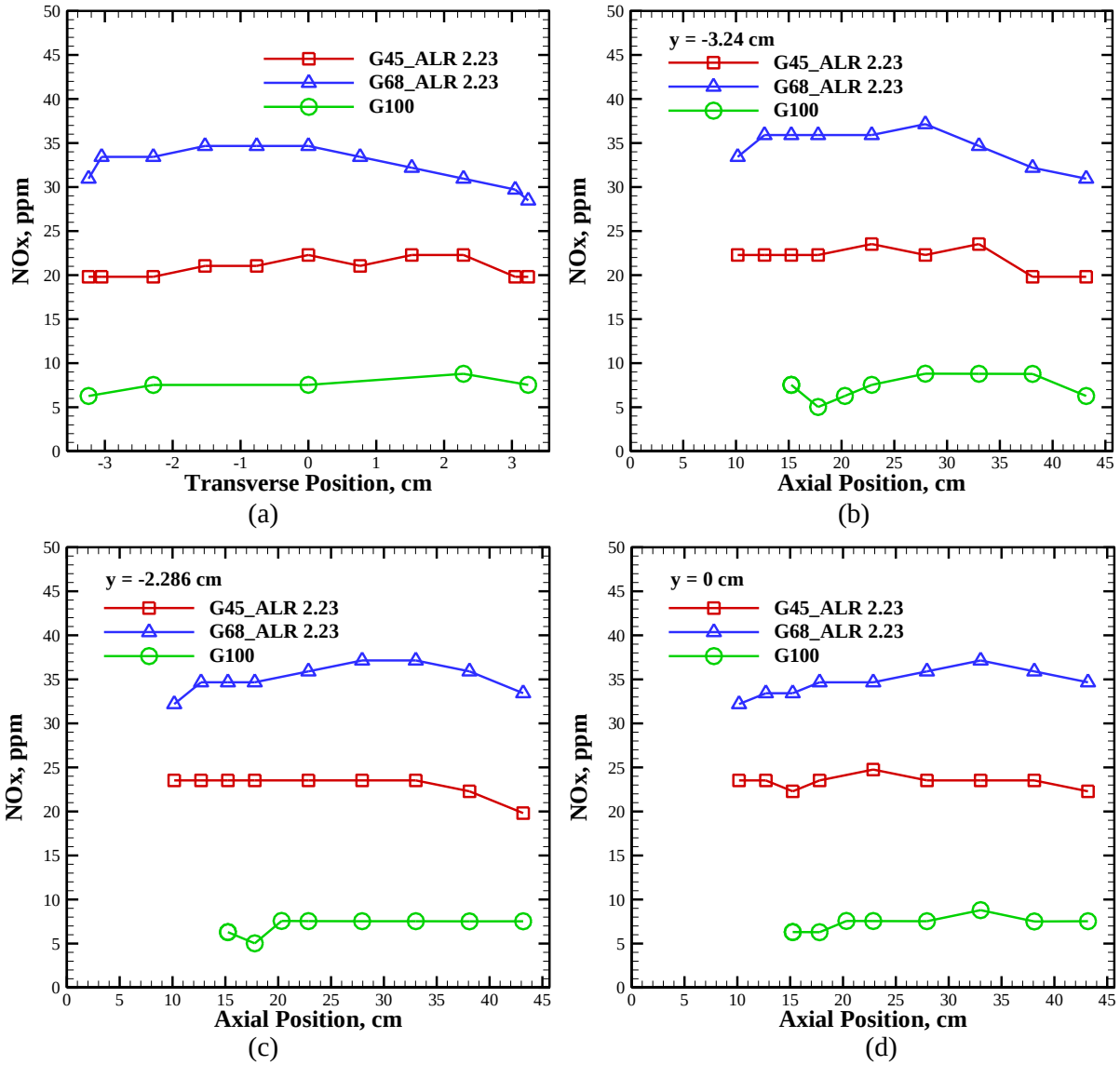

Fig. 9 NOx concentrations in the combustor for different fuel composition.

Fig. 8(a) compares the radial profiles of CO emissions at the combustor exit. For all three flames, the CO emissions in the 2-digit ppm range which is very low. Emissions are lowest in the center region and they increase near the wall where thermal quenching would take place. For G100 flame, much higher CO emissions near the wall could result from larger droplet hitting the wall and combusting only partially. Figs. 8(b)-(d) show axial profiles of CO emissions at several transverse locations in the combustor. G45 and G68 flames show extremely low CO emissions throughout the

combustor, which is consistent with the reaction zone located closer to the injector exit. G100 flame has generally higher CO emissions at the combustor center CO emissions, decreasing in the flow direction where oxidation reactions take place. However, CO emissions at y = -3.24 cm or near the wall increase in the flow direction, suggesting that larger droplets reaching the combustor periphery might not undergo complete combustion. This situation can be avoided by utilizing thermal feedback from combustion of small amounts methane introduced in the combustor. In any case, results demonstrate that with FB injector it is possible to cleanly burn glycerol without heating or pre-processing it.

Fig. 9(a) shows the radial profile of NO_x emissions at the combustor exit plane and Fig. 9(b)-(d) show the axial profiles of NO_x emission at various transverse locations for the three flames. Emissions samples were taken between z = 10 cm and combustor exit plane. NO_x emissions, favoring the high temperature mechanism, are higher for flames with methane as part of the fuel than those from the single fuel (glycerol) combustion. Local NO_x emissions from G45 flame are lower than those from G68 flame. This result is explained by the shorter high temperature reaction zone of the G45 flame. For G100 flame, the reaction extends the length of the combustor however reaction zone temperatures are also lower. Thus, the resulting NO_x emissions for G100 flame are much lower than those from methane containing G45 and G68 flames. Still, the NO_x emission levels are very low for all three flames, and demonstrate the fuel flexible nature of the FB injector.

3.2. Effect of Air to Liquid Mass Ratio (ALR)

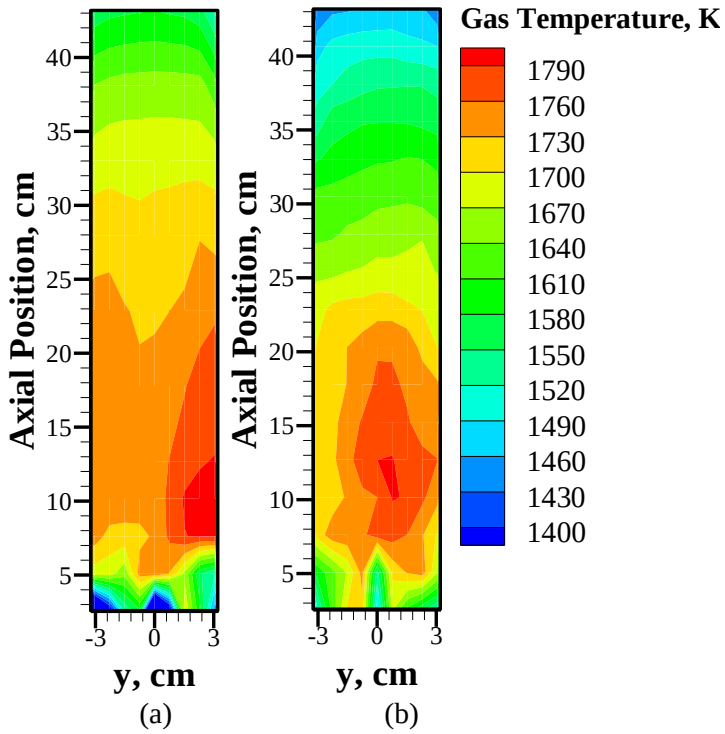

Fig. 10 Gas temperature contour inside the combustor for (a) G68_ALR 1.47 and (b) G68_ALR 2.23.

ALR does not affect the mean surface temperature of the combustor for G68 flames for fixed HRR as shown in Fig. 5(b). Fig. 10 shows contours of temperatures (uncorrected) inside the combustor for G68 flames with different ALRs. The reaction zone for ALR = 2.23 flame is shorter

and closer to the injector exit compared to the ALR = 1.47. This result is the direct outcome of the fuel-atomization, pre-vaporization, and fuel-air mixing processes, which are more effective for the higher ALR case. Consequently, reactions occur earlier in the high ALR flame releasing heat near the injector which further improves fuel pre-vaporization in return. Downstream of the reaction zone, temperature decreases in the flow direction because of heat loss from the combustor wall.

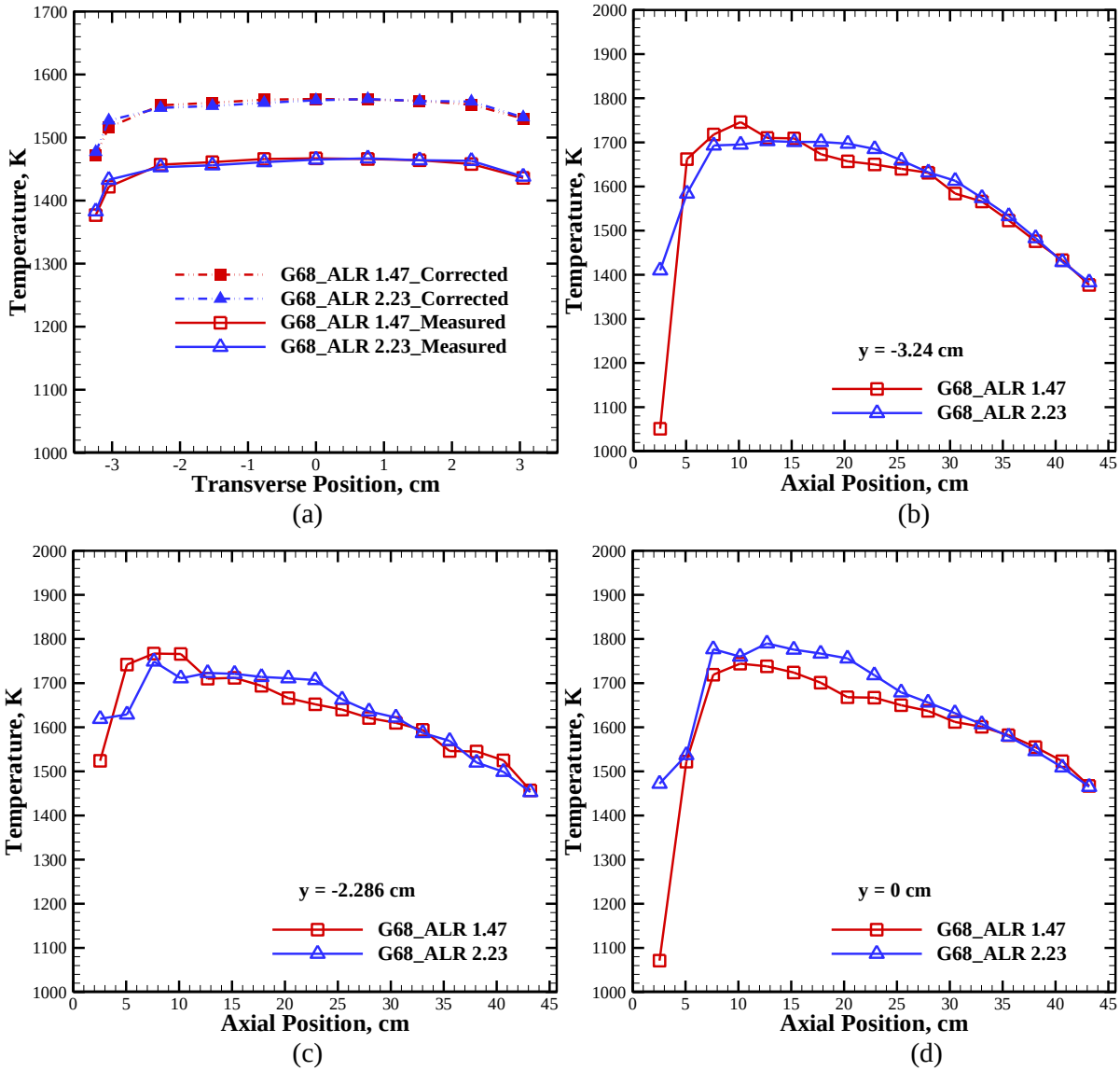

Fig. 11 Gas temperatures in the combustor for different ALRs with the same fuel composition.

Fig. 11(a) illustrates the effect of ALR on transverse profiles of uncorrected and radiation-corrected gas temperature; note that the temperature correction is about 94 K for both cases. Axial profiles of gas temperature in Figs. 11(b)-(d) show higher gas temperature in the very near field Z < 5 cm for higher ALR case compared to lower ALR case, indicating faster vaporization for the former case. In contrast, near the wall, slightly higher temperature is observed for the ALR = 1.47 flame. The likely reason is the greater number of larger droplets associated with the low ALR reaching the wall and combusting in diffusion mode. In general, differences in temperature distribution within the combustor have negligible effect on product gas temperature at the combustor exit.

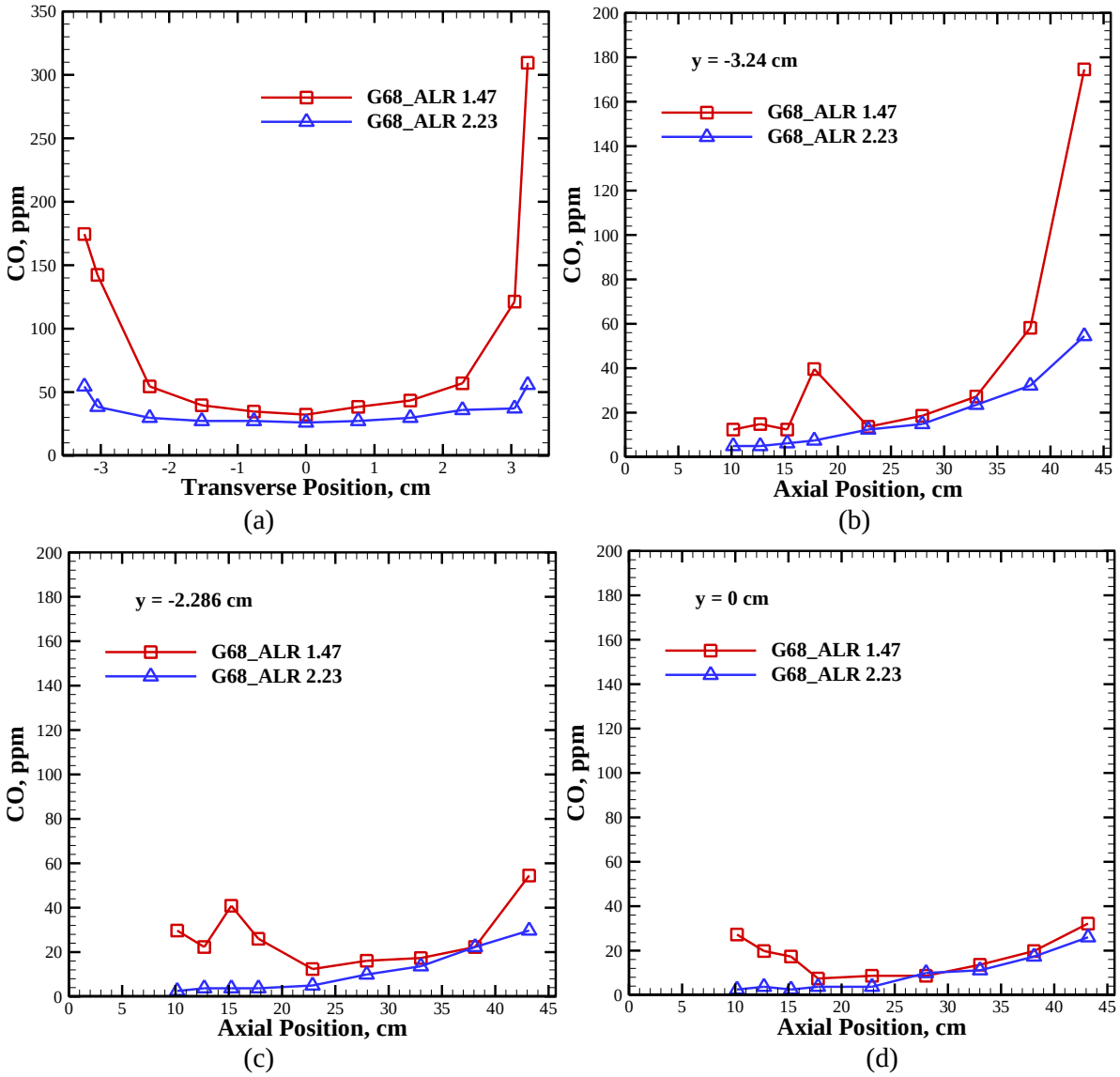

Fig. 12 CO concentrations in the combustor for different ALRs with the same fuel compostion.

Fig. 12(a) compares the radial profiles of CO emissions at the combustor exit to reveal the ALR effect for G68 flames. For both ALRs, CO emissions are low in the center region and increase towards the wall as discussed previously. For ALR = 1.47, CO emissions near the wall are much higher than those in the center region indicating larger droplets reaching the wall and burning partially and/or in diffusion mode. Fig. 12(b)-(d) show axial profiles of CO concentrations at different radial locations for the two flames. For both cases, CO concentrations from the two ALRs are low. CO concentrations for high ALR flame are lower mainly because of the higher local gas temperatures. For all cases, the spacially-averaged CO levels are low.

Fig. 13(a) shows the ALR effect on the radial profile of NO_x emissions at the combustor exit plane and Fig. 13(b)-(d) show the axial profiles of NO_x emission at various transverse locations for different ALRs. NO_x emissions are relatively higher for the higher ALR case, which is consistent with temperature measurements. Finer droplets produced for higher ALR case are vaporized fast and mix quickly with air to release heat in a relative intensified region with higher local temperatures. Overall, for both ALRs, NO_x emissions are low indicating good atomization by FB

injector. Further improvements in emissions performance could be achieved by optimizing geometric parameters (D and/or H) of the injector.

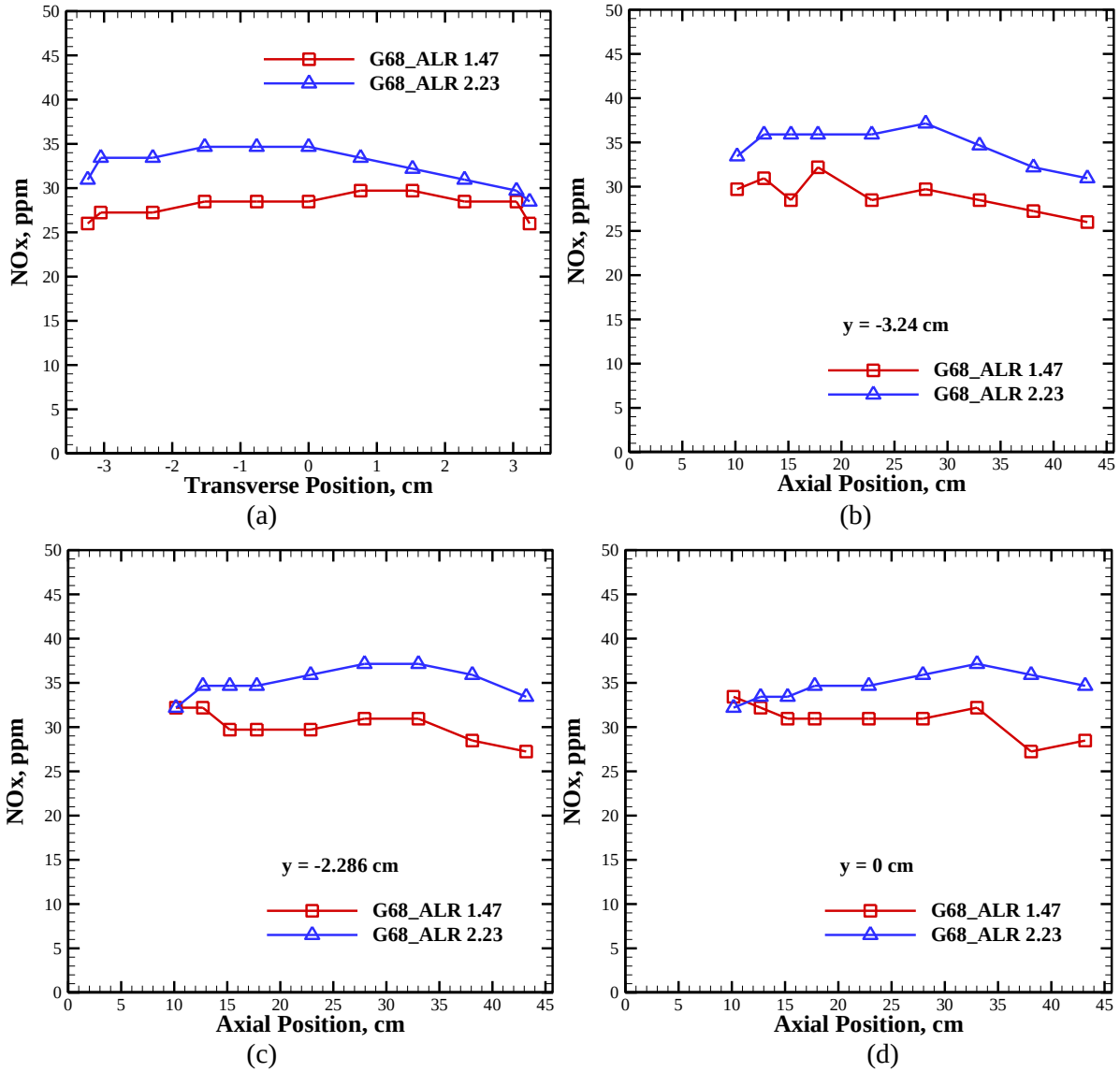

Fig. 13 NOx concentrations in the combustor for different ALRs with the same fuel compostion.

3.3. Droplet size and lifetime characteristics

As discussed above, all of the flames investigated with FB injector are clean producing low CO and NOx emissions. Introduction of methane in the combustor improves pre-vaporization of glycerol droplets produced by the injector. Detailed measurements by Simmons et al [10] using a Phase Doppler Particle Analyzer (PDPA) showed that glycerol droplets produced by FB atomizer have flow-weighted Sauter Mean Diameters (SMD) of 35μm and 40 μm at z = 10 cm, respectively for G48 and G68 flames. These results are introduced to further evaluate the evaporation time and the critical diameter (D_c) of the droplets using a simple droplet lifetime model [18]. The critical diameter is defined as the maximum diameter of the droplet which can completely evaporate in the pre-vaporization and fuel-air mixing zone near the injector orifice. The axial velocity of 12 m/s previously measured for most of the droplets is utilized to predict D_c for the three fuels [18]. The

length of the pre-vaporization and fuel-air mixing zone of 10 cm, according to the gas temperature contours in Fig. 6 and Fig. 10, is chosen for the approximate evaluation. For G45 flame, the temperature in the glycerol vaporization zone is as high as 1600 K to 1800 K as shown in Fig. 6. In G68 flame, the temperature varies from 1000 K to 1800 K as shown in Fig. 10.

Fig. 14 illustrates the maximum diameter of the glycerol droplets that would evaporate completely in the pre-vaporization for the present study. Evidently, for G45 flame, droplets of around 35 µm, containing most of the fuel mass, are smaller than the critical droplet diameter D_c. Thus, complete pre-vaporization of most of glycerol can be expected to occur before combustion in the near field. For G68 flame, when pre-vaporization zone temperature is below 1280 K, droplets of 40 µm diameter could not evaporate completely. From Fig. 10, it is evident that methane combustion results in reaction zone temperature of up to 1800 K, which is sufficient to completely pre-vaporize glycerol droplets. This simple analysis suggests that glycerol droplets with most of the fuel mass would pre-vaporize and burn in premixed combustion mode to yield low CO and NOx emission.

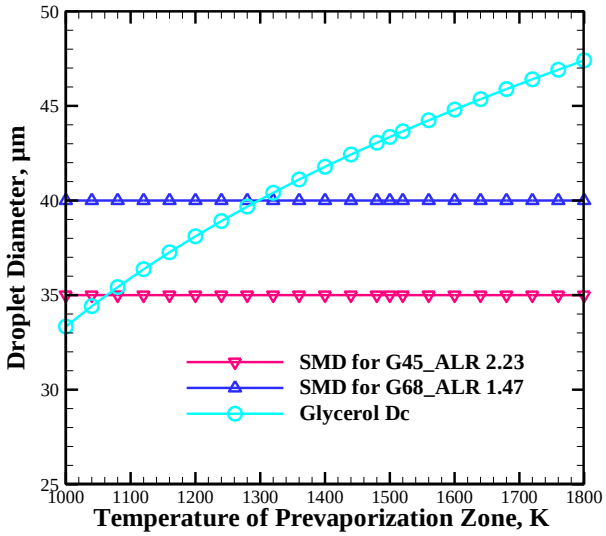

Fig. 14 Critical droplet diameters based on the prevaporization zone length (PZL) of 10 cm at droplet RMS axial velocity of 12m/s.

4. Conclusions

In this study, low-emission combustion of glycerol/methane has been achieved by utilizing a fuel-flexible FB injector to yield fine droplets of highly viscous glycerol. Heat released from methane combustion further improves glycerol pre-vaporization and thus its clean combustion. Methane addition results in an intensified reaction zone with locally high temperatures near the injector exit. Reduction in methane flow rate elongates the reaction zone, which leads to higher CO emissions and lower NO_x emissions. Similarly, higher ALR improves atomization and fuel pre-vaporization and shifts the flame closer to the injector exit. In spite of these internal variations, all fuels produced similar CO and NO_x emissions at the combustor exit. Results show that FB concept provides low emissions with the flexibility to utilize gaseous and highly viscous liquid fuels that are difficult to atomize using conventional techniques.

Acknowledgments

This research was supported by the US Department of Energy Award EE0001733.

References

[1] Dasari, M.A., P.P. Kiatsimkul, W.R. Sutterlin, and G.J. Suppes, "Low-pressure hydrogenolysis of glycerol to propylene glycol," *Applied Catalysis A: General*, Vol. 281, No. 1-2, 2005, pp. 225-231.

[2] Demirbas, A., "Conversion of biomass using glycerin to liquid fuel for blending gasoline as alternative engine fuel," *Energy Conversion and Management*, Vol. 41, No. 16, 2000, pp. 1741-1748.

[3] Naresh Pachauri, Brian He, "Value-added Utilization of Crude Glycerol from Biodiesel Production: A Survey of Current Research Activities", *ASABE Meeting Paper No*. 066223, Portland, Oregon, 2006.

[4] Wang, K., M.C Hawley, and S.J. DeAthos, "Conversion of glycerol to 1,3-propanediol via selective dehydroxylation," *Industrial and Engineering Chemistry Research*, Vol. 42, No. 13, 2003, pp. 2913-2923.

[5] Ito, T., Y. Nakashimada, K. Senba, T.Matsui, and N. Nishio, "Hydrogen and ethanol production from glycerol-containing wastes discharged after biodiesel manufacturing process," *Journal of Bioscience and Bioengineering*, Vol. 100, No. 3, 2005, pp. 260-265.

[6] López, J., Santos, M., Pérez, M. and Martín, M., "Anaerobic digestion of glycerol derived from biodiesel manufacturing," *Bioresour. Technol.*, Vol. 100, 2009, pp. 5609–5615.

[7] McNeil, John, Day, Paul and Sirovski, Felix, "Glycerine from biodiesel: The perfect diesel fuel," *Process Safety and Environmental Protection*, Vol. 90, No. 3, 2012, pp. 180-188.

[8] B. Metzger, "Glycerol Combustion," *M.S. Thesis*, Mechanical Engineering Dept., North Carolina State University, 2007.

[9] Myles D. Bohon, Brian A. Metzger, William P. Linak, Charly J. King and William L. Roberts, *Proceedings of the Combustion Institute*, Vol. 33, 2010, pp. 2717–2724.

[10] Simmons, B.M., "Atomization and Combustion of Liquid Biofuels," *Ph.D. Dissertation*, Mechanical Engineering Dept., Univ. of Alabama, Tuscaloosa, AL, 2011.

[11] Alfonso M. Gañán-Calvo, "Enhanced liquid atomization: From flow-focusing to flow-blurring," *Applied Physics Letters*, Vol. 86, No. 21, AIAA, Sevilla, Spain, 2005, pp. 2141-2142.

[12] Lulin Jiang, Pankaj S. Kolhe, Robert P. Taylor, and Ajay K. Agrawal, 2012, "Scalar Measurements in a Combustor Operated on Alternative Liquid Fuels", *51st AIAA Aerospace Sciences Meeting Including the New Horizons Forum and Aerospace Exposition*, January 9-12, Nashville, Tennessee.

[13] Simmons, B.M., Panchasara, H.V. and Agrawal, A.K., "A comparison of air-blast and flow blurring injectors using phase Doppler particle analyzer techniques," *ASME Conference Proceedings*, 2009 (48838), pp. 981-992.

[14] Simmons, B.M. and Agrawal, A. K., "Spray characteristics of a flow blurring atomizer," *Atomization and Sprays*, Vol. 20, No. 9, 2010, pp. 821-825.

[15] Panchasara, H., Sequera, D., Schreiber, W. and Agrawal, A.K., "Combustion performance of a novel injector using flow-blurring for efficient fuel atomization," *Journal of Propulsion and Power,* Vol. 25, No. 4, 2009, pp. 984-987.

[16] Benjamin M Simmons and Ajay K. Agrawal, "Flow Blurring Atomization for Low-Emission Combustion of Liquid Biofuels," *Combustion Science and Technology*, Vol. 184, No. 5, pp. 660-675.

[17] Benjamin M. Simmons, Pankaj S. Kolhe, Robert P. Taylor, and Ajay K. Agrawal, "Glycerol Combustion using Flow-Blurring Atomization," *the 2010 Technical Meeting of the Central States Section of The Combustion Institute*, Champaign, Illinoi, 2010.

[18] Turns, S.R., *An Introduction to Combustion Concepts and Applications*, 2nd ed., McGraw-Hill Higher Education, USA, 2000, pp. 376-378.